Coherence Resonance and Stochastic Resonance in an Excitable Semiconductor Superlattice

Emanuel Mompo,[1] Miguel Ruiz-Garcia,[1] Manuel Carretero,[1] Holger T. Grahn,[2] Yaohui Zhang,[3,4] and Luis L. Bonilla[1,*]

[1]*Gregorio Millán Institute for Fluid Dynamics, Nanoscience and Industrial Mathematics, and Department of Materials Science and Engineering and Chemical Engineering, Universidad Carlos III de Madrid, 28911 Leganés, Spain*

[2]*Paul-Drude-Institut für Festkörperelektronik, Leibniz-Institut im Forschungsverbund Berlin e. V., Hausvogteiplatz 5–7, 10117 Berlin, Germany*

[3]*Key Laboratory of Nanodevices and Applications, Suzhou Institute of Nano-Tech and Nano-Bionics, Chinese Academy of Sciences, Suzhou 215123, China*

[4]*College of Liberal Arts and Sciences, National University of Defense Technology, Changsha 410073, China*

(Received 19 December 2017; published 24 August 2018)

Collective electron transport causes a weakly coupled semiconductor superlattice under dc voltage bias to be an excitable system with $2N + 2$ degrees of freedom: electron densities and fields at N superlattice periods plus the total current and the field at the injector. External noise of sufficient amplitude induces regular current self-oscillations (coherence resonance) in states that are stationary in the absence of noise. Numerical simulations show that these oscillations are due to the repeated nucleation and motion of charge dipole waves that form at the emitter when the current falls below a critical value. At the critical current, the well-to-well tunneling current intersects the contact load line. We have determined the device-dependent critical current for the coherence resonance from experiments and numerical simulations. We have also described through numerical simulations how a coherence resonance triggers a stochastic resonance when its oscillation mode becomes locked to a weak ac external voltage signal. Our results agree with the experimental observations.

DOI: 10.1103/PhysRevLett.121.086805

Constructive effects of noise include superresolution in time reversal acoustics [1,2], signal enhancement due to stochastic resonance (SR) [3–6], coherence resonance (CR) [7–10], etc. In nonlinear excitable systems [11], noise of appropriate strength can trigger coherent oscillations (CR) and enhance the signal-to-noise ratio of a periodically driven bistable system (SR). These constructive effects of noise are typically demonstrated in few-degrees-of-freedom systems amenable to analytical and simple numerical studies, e.g., a particle in a double-well potential under white noise and ac driving forces in the SR case [4] and an excitable system described by the FitzHugh-Nagumo equation in the CR case [8,9].

Technologically relevant devices are often complex and harder to characterize, yet they may exhibit CRs as well as SRs. A case in point are excitable semiconductor superlattices (SSLs). Because of sequential tunneling electron transport (STET), voltage-biased, doped, weakly coupled SSLs can be modeled as nonlinear systems with many degrees of freedom. They exhibit excitable or oscillatory behavior depending on the driving and configuration parameters [12,13]. For large doping densities, SSLs have multistable stationary states that produce sawtooth-like current-voltage characteristics under dc voltage bias. A square voltage pulse may induce excitability [14] visualized by a large current spike caused by the formation at the cathode and motion towards the anode of a charge dipole wave (CDW) [13,15]. After the wave disappears, there remains a stable static state consisting of a lower electric-field domain near the cathode followed by a higher field domain that extends to the anode. For lower doping densities, the SSL total current (TC) may oscillate periodically in time due to repeated CDW formation and motion [13]. Depending on the cathode conductivity, doping density, and temperature, voltage intervals of stable stationary states may be followed by intervals of stable oscillatory states [10]. Based on numerical simulations, a CR has been predicted [10] and observed in experiments on GaAs/AlAs SL at low temperatures [16].

Recently, under dc voltage bias, spontaneously chaotic [17,18], periodic, and quasiperiodic [19] self-sustained current oscillations have been observed in $GaAs/Al_{0.45}Ga_{0.55}As$ 50-period SLs at room temperature. Noise may induce or enhance chaotic oscillations over a wider voltage bias range provided its amplitude is sufficiently large and its bandwidth is much smaller than the oscillation frequency [20]. Numerical simulations show that thermal and shot noise enhance deterministic spontaneous chaos in a STET model of a SSL of 50 identical spatial periods [21,22]. For shorter SSLs, theory predicts enhanced deterministic chaos due to a

Feigenbaum period-doubling cascade in certain voltage intervals [23]. Reference [24] studies how variations in basic design parameters influence chaos.

In this Letter, we study the CR in dc voltage-biased SSLs at room temperature driven by external noise having a bandwith larger than the oscillation frequency. We also study the SR when a small ac voltage is added. The corresponding experimental results are presented in Ref. [25]. For a dc voltage bias, when the current drops below a critical value, the external noise may produce large current spikes due to the formation of a CDW at the injector that propagates toward the collector and disappears there. The value of the critical TC (CTC) to trigger a CDW is given by the intersection of the well-to-well sequential current density with the injector load line (current density versus local electric field). Both these device-specific functions cannot be directly determined from experiments. However, the CTC can be extracted from numerical simulations of the theoretical model by studying the ratio of the standard deviation to the mean duration of large current spikes. As the noise amplitude increases, a coherent oscillation develops, which corresponds to a minimum of the standard deviation of interspike time intervals divided by the mean interspike time. Similar to this numerically demonstrated CR, noise may enhance a weak ac signal, thereby demonstrating a SR. Experiments confirm these predictions [25].

Model.—The electric field $-F_i$ and the two-dimensional electron density n_i at well i ($i = 1, \ldots, N$) satisfy [12,13,22,26–28]

$$\epsilon \frac{dF_i}{dt} + J_{i\to i+1} = J(t), \tag{1}$$

$$n_i = N_D + \frac{\epsilon}{e}(F_i - F_{i-1}), \tag{2}$$

where $-e < 0$, ϵ, N_D, $J(t)$ and $J_{i\to i+1}$ are the electron charge, SSL average permittivity, doping density, TC density, and tunneling current density from well i to $i+1$, respectively [12,13,22]:

$$J_{i\to i+1} = \frac{en_i}{l} v^{(f)}(F_i) - J^{-}_{i\to i+1}(F_i, n_{i+1}, T), \tag{3}$$

$$J^{-}_{i\to i+1}(F_i, n_{i+1}, T) = \frac{em^* k_B T}{\pi\hbar^2 l} v^{(f)}(F_i) \times \ln\left[1 + e^{-\frac{eF_i l}{k_B T}}\left(e^{\frac{\pi\hbar^2 n_{i+1}}{m^* k_B T}} - 1\right)\right]. \tag{4}$$

The function $v^{(f)}(F_i)$ has peaks corresponding to the discrete energy levels in every well [12,13,22] (45, 173, and 346 meV, for a 7 nm GaAs/4 nm $Al_{0.45}Ga_{0.55}As$ SL [17,18,20,25]). The barrier height is 388 meV. The mesa cross section is a square with a 30 μm side length and $N = 50$ [25]. m^*, l, k_B, T are the average effective mass, SSL period, Boltzmann constant, and lattice temperature, respectively [12]. Voltage bias and boundary conditions are [12,13,20,22,27,29]

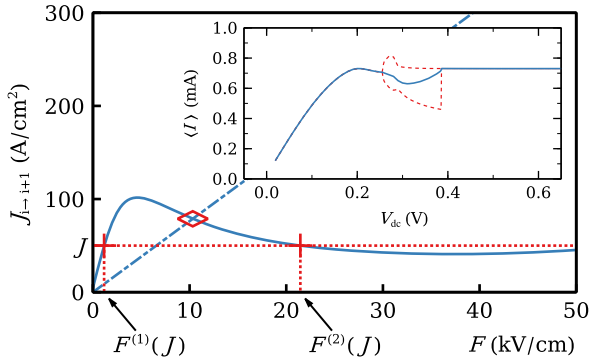

FIG. 1. Current-field characteristics (solid line) and injector load line (dot-dashed line) for $F_i = F$ and $n_i = N_D$. The first intersection point yields the CTC (rhombus), $J_{cr} = 78.7959$ A/cm^2 and field, $F_{cr} = 10.3265$ kV/cm. Inset: $I - V$ characteristics indicating maximum and minimum values of the current in the oscillatory regime (dotted lines).

$$l\sum_{i=1}^{N} F_i = V + \eta(t), \qquad \eta(t) = \eta_{th}(t) + \eta_c(t), \tag{5}$$

$J_{0\to 1} = \sigma_0 F_0$ and $J_{N\to N+1} = \sigma_0 (n_N/N_D) F_N$. Figure 1 shows the tunneling current density versus the constant field $F_i = F$ for $n_i = N_D$ and also the injector load line (dot-dashed line). In Eq. (5), the voltage V may comprise the dc voltage bias V_{dc} and an ac signal $V_{ac} = V_{sin}\sin(2\pi\nu t)$. The voltage noise $\eta(t)$ has two components: (i) $\eta_{th}(t)$, which is related to the noise of the source, and (ii) the external noise $\eta_c(t)$. $\eta_{th}(t)$ is simulated by picking random numbers every 5×10^{-11} s from a zero mean distribution with a standard deviation of 2 mV [20]. $\eta_c(t)$ is a white noise with bandwidth of 1 GHz and tunable amplitude V^{rms}_{noise}. These noise values have been selected so that the results of the numerical simulations of the model agree qualitatively with the results of the experiments reported in Refs. [20,25]. We have ignored the smaller value of $\eta_{th}(t)$ at the SSL wells [21,22].

Results.—Equations (1)–(5) yield predictions that are in *qualitative agreement* with experiments. Typically the TC and the frequency of TC self-oscillations (TCSO) are lower than observed [13], which we shall consider when comparing with experiments. For deterministic dc voltage bias, TCSO begin as a supercritical Hopf bifurcation at $V_{dc} = 0.255$ V and end at a saddle-node, infinite-period bifurcation (SNIPER) at $V_{dc} = 0.385$ V (cf. inset of Fig. 1). The experiments exhibit the same scenario [25].

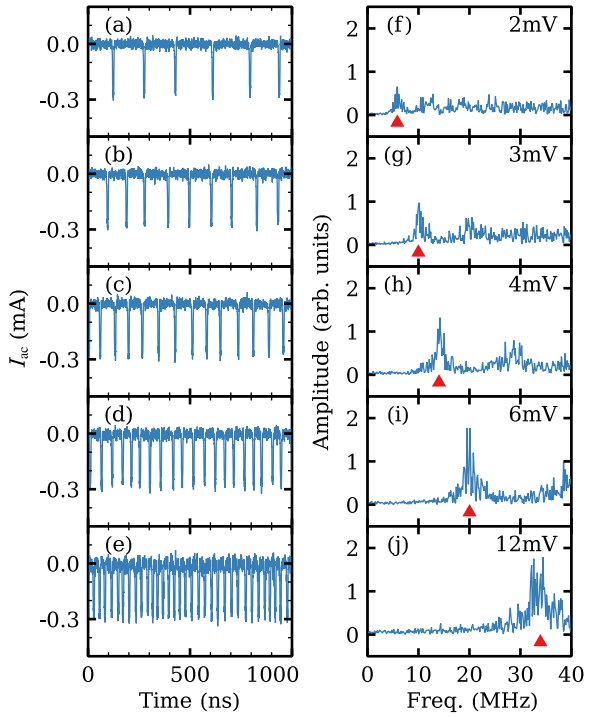

FIG. 2. Coherence resonance: (a)–(e) ac components of the TC versus time and (f)–(j) corresponding frequency spectra (interspike average frequency marked by a triangle) for different noise amplitudes at $V_{dc} = 0.387$ V. Values of V_{noise}^{rms} are 2, 3, 4, 6, and 12 mV. Current traces have been shifted to have zero current at the stationary state.

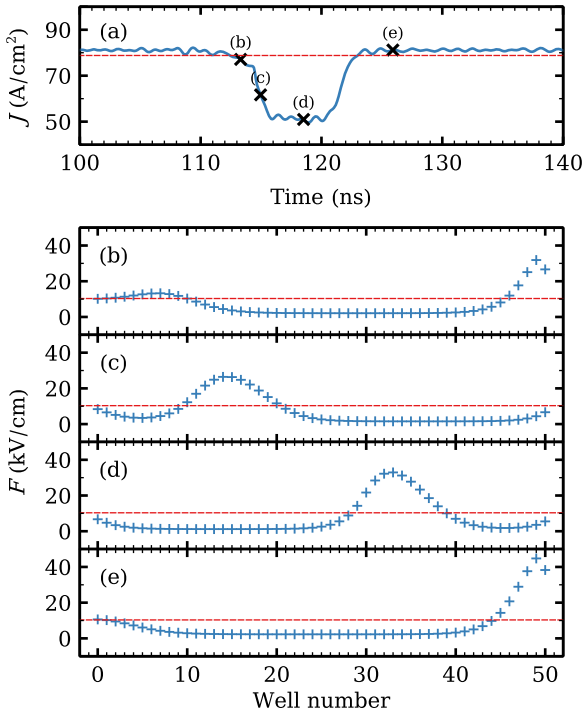

FIG. 3. (a) TC density versus time for $V_{dc} = 0.387$ V, $\eta_{th} = 0$, and $V_{noise}^{rms} = 3$ mV. (b)–(e) Field profiles at the times marked in (a). Dashed lines indicate the critical current and field. See also movie in the Supplemental Material [28].

Adding noise with increasing amplitude at $V_{dc} = 0.387$ V, TCSO appear as shown in Figs. 2(a)–2(e) for $V_{noise}^{rms} > 1.4$ mV indicating the presence of a CR. The CR frequency follows the interspike average frequency [marked by triangles in Figs. 2(f)–2(j)], which increases with increasing V_{noise}^{rms}. For $V_{noise}^{rms} < 2$ mV, the TC presents a rapid small-amplitude oscillation (caused by the noise) and large spikes separated by long-time intervals. Between spikes, the TC is close to a constant value slightly above J_{cr} defined in Fig. 1. Figure 3(a) shows an enlarged view of $J(t)$ for an interval containing one large current spike with field profiles shown in Figs. 3(b)–3(e). Outside the spike, the corresponding field profile is quasistationary [cf. Fig. 3(e)]: $F_i \approx F_{cr}$ near the injector, then F_i decreases to $F^{(1)}(J)$, stays there for several periods, and increases again near the collector. As shown in Figs. 3(b)–3(d), each large current spike corresponds to CDW creation and motion when J decreases and stays below J_{cr} for some time. As $J < J_{cr}$, the high-field region near the collector tries to move out leaving a field $F^{(1)}(J)$ on its wake. However, the total area under the electric field profile is conserved on average according to Eq. (5). As the pulse near the collector departs, the lost area has to be compensated by launching a new CDW at the injector, which causes the TC to decrease as Figs. 3(a)–3(c) show. When the CDW arrives at the collector and starts disappearing, J increases up to its stationary value (except for noise-produced small-amplitude oscillations), and F_i becomes quasistationary [cf. Fig. 3(e)].

Figure 4 depicts the normalized standard deviation $R_{T_a} = \sqrt{\langle T_a^2 \rangle - \langle T_a \rangle^2}/\langle T_a \rangle$ of the interspike time interval, T_a, versus V_{noise}^{rms}. It exhibits a minimum after an abrupt drop followed by a smooth increase. This behavior is expected for voltages close to a SNIPER bifurcation [10].

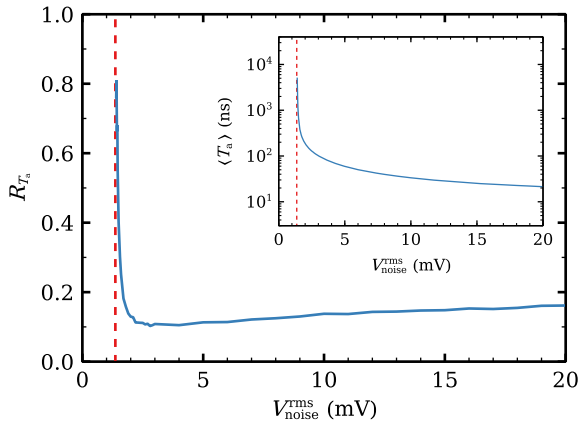

FIG. 4. Normalized standard deviation R_{T_a} versus V_{noise}^{rms} ($\eta_{th} = 0$). Inset: mean interspike interval $\langle T_a \rangle$ versus V_{noise}^{rms}. The vertical asymptotes (dashed lines) occur at $V_{noise}^{rms} = 1.365$ mV.

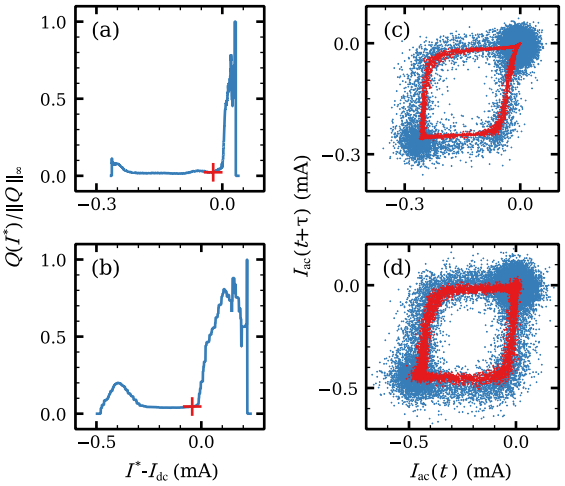

FIG. 5. Normalized standard deviation to mean ratio of large current spike duration, $Q(I^*)$, versus $I^* - I_{dc}$ for a CR from: (a) numerical simulations with $V_{dc} = 0.387$ V, $\eta_c = 6$ mV, and $\eta_{th} = 0$; (b) experimental data with $V_{dc} = 0.773$ V and $V_{noise}^{rms} = 8.288$ mV. The crosses in (a) and (b) mark I_{cr}. Standard deviations and means are taken over the union set of all disjoint time intervals lasting more than t^* (one third of the average duration of a large current spike) during which the current is $I(t) < I^*$. Simulations and experimental data yield $t^* = 10$ and 3 ns, respectively. Attractor of the CR in the $(I_{ac}(t), I_{ac}(t+\tau))$ phase plane of embedded coordinates [30]: (c) numerical simulations with $V_{dc} = 0.387$ V, $\tau = 1.642$ ns, $\eta_c = 8$ mV, $\eta_{th} = 2$ mV; (d) experimental data with $\tau = 0.884$ ns and other parameters as in (b). The sharper red attractors in (c) and (d) are obtained by noise filtering with a 8-level Haar wavelet [31].

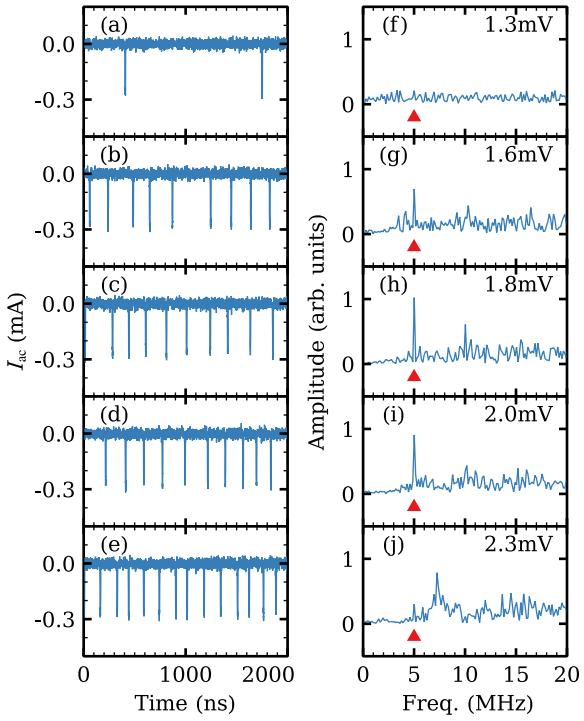

FIG. 6. Stochastic resonance: (a)–(e) ac components of the SSL current versus time and (f)–(j) corresponding frequency spectra (frequency of ac signal marked by a triangle) for different noise amplitudes at $V_{dc} = 0.387$ V and a sinusoidal ac signal of frequency $\nu = 5$ MHz and $V_{sin} = 0.646$ mV. The values of V_{noise}^{rms} are 1.4, 1.7, 1.9, 2.1, and 2.3 mV.

The mean interspike interval $\langle T_a \rangle$ shown in the inset of Fig. 4 first decreases from infinity at $V_{noise}^{rms} = 1.365$ mV and rather more smoothly for $V_{noise}^{rms} > 2$ mV. This behavior is typical of a CR and agrees qualitatively with the experimental results [25].

We now estimate the CTC for triggering new pulses by comparing experimental with simulated results. This device-dependent quantity (cf. Fig. 1) has great importance for theory. We select data at voltages slightly larger than the SNIPER bifurcation, 0.387 V (theory) and 0.773 V (experiments) [25]. The larger experimental value is due to voltage drops at the contact region and at the 50 Ohm impedance of the oscilloscope. The stationary state TC is obtained as the average current between two large spikes when the external noise is so low that few large spikes exist. For the model, we know the CTC exact value, 0.709 mA, which is 97% of the stationary state TC. From the experiments, 97% of the stationary state TC (1.448 mA) is 1.404 mA, which is our estimated CTC. This value is confirmed by comparing the theoretical and experimental normalized ratio of the standard deviation of the duration of large long-lasting current peaks to their mean duration. Figure 5 shows this comparison. The normalized ratio versus current, CTC location, and even the shape of the CR attractor are qualitatively quite similar (cf. Ref. [28]).

Figures 6(a)–6(e) show the result of adding a small amplitude ac signal to the dc voltage with a frequency within the CR range and then increasing the noise amplitude. Isolated current spikes separated irregularly by long intervals appear for $V_{noise}^{rms} < 1.4$ mV. With increasing noise amplitudes, the SSL oscillates at a frequency locked with that of the ac signal, as shown in Figs. 6(g)–6(i). At larger V_{noise}^{rms}, the main frequency increases and ceases to be locked to that of the ac signal, as shown in Fig. 6(j). This is the signature of a SR. Figures 7(a) and 7(b) show the output signal-to-noise ratio SNR_{out} and the gain of the signal-to-noise ratio $SNR_{gain} = SNR_{out}/SNR_{in}$, respectively, of the SSL under SR [28]. Experiments confirm that this SR exists [25]. However, the enhancement of the signal-to-noise ratio (more than 100 dB) is larger in the simulations than that observed in experiments (more than 30 dB) [25], not surprisingly as our idealized model does not include many noise sources of the actual experimental setup. As shown in the inset of Fig. 7(b), the necessary noise amplitude for frequency locking is smaller than that needed for a CR when $V_{sin} = 0$. V_{noise}^{rms} decreases with V_{sin}, as observed in the experiments [25].

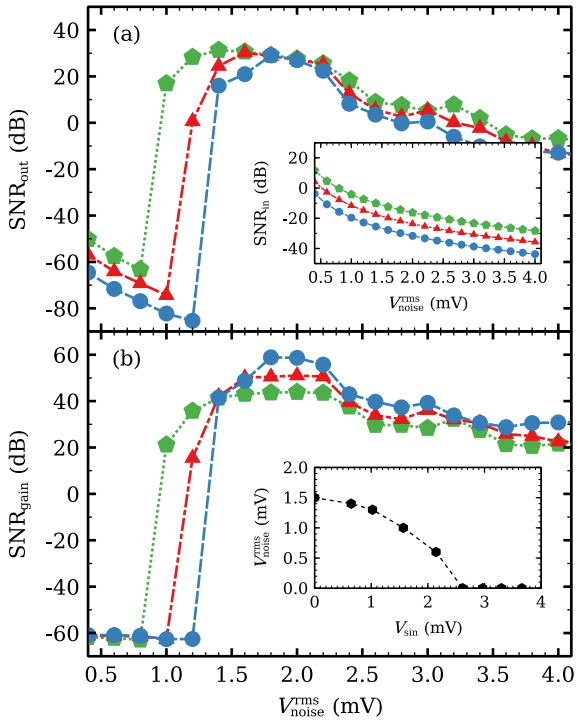

FIG. 7. (a) SNR_{out} (inset: SNR_{in}) and (b) SNR_{gain} versus V_{noise}^{rms} (varied from 0.5 to 4 mV) for $V_{sin} = 0.646$ (circles), 1.022 (triangles), and 1.736 mV (pentagons). The inset of (b) shows the values of V_{noise}^{rms} needed to trigger periodic TCSO versus V_{sin}.

In conclusion, by numerical simulations of a STET model of SSLs at room temperature, we have found a CR and a SR. The CR is due to repeated and coherent generation of CDWs at the injector when the amplitude of external noise surpasses a certain threshold. For the first time, we have estimated the value of the critical current necessary to trigger waves from experimental data. When we add an external ac signal with a frequency within that of the CR, the SSL phase locks to the ac signal, even if the latter is weak [28]. Our simulations agree qualitatively with the experimental results [25] and confirm that SSLs under SR can act as lock-in amplifiers.

The authors thank the Ministerio de Economía y Competitividad of Spain (Grants No. MTM2014-56948-C2-2-P and No. MTM2017-84446-C2-2-R), the Strategic Leading Science and Technology Special Program of the Chinese Academy of Sciences (Grant No. XDA06010705), the National Natural Science Foundation of China (Grants No. 61070040 and No. 61204093), the National Key Research and Development Program of China (Grant No. 2016YFE0129400), and the Exploration Project (Grant No. 7131266) for financial support. E. M. acknowledges support from the Ministerio de Economía y Competitividad of Spain through the Formación de Doctores program cofinanced by the European Social Fund. M. R.-G. acknowledges support from Ministerio de Educación, Cultura y Deporte of Spain through the Formación de Profesorado Universitario program.

*bonilla@ing.uc3m.es

[1] A. Derode, P. Roux, and M. Fink, Phys. Rev. Lett. **75**, 4206 (1995).
[2] P. Blomgren, G. C. Papanicolaou, and H. Zhao, J. Acoust. Soc. Am. **111**, 230 (2002).
[3] B. McNamara, K. Wiesenfeld, and R. Roy, Phys. Rev. Lett. **60**, 2626 (1988).
[4] L. Gammaitoni, P. Hänggi, P. Jung, and F. Marchesoni, Rev. Mod. Phys. **70**, 223 (1998).
[5] R. L. Badzey and P. Mohanty, Nature (London) **437**, 995 (2005).
[6] P. S. Burada, G. Schmid, D. Reguera, M. H. Vainstein, J. M. Rubí, and P. Hänggi, Phys. Rev. Lett. **101**, 130602 (2008).
[7] G. Hu, T. Ditzinger, C. Z. Ning, and H. Haken, Phys. Rev. Lett. **71**, 807 (1993).
[8] A. S. Pikovsky and J. Kurths, Phys. Rev. Lett. **78**, 775 (1997).
[9] R. E. Lee DeVille, E. Vanden-Eijnden, and C. B. Muratov, Phys. Rev. E **72**, 031105 (2005).
[10] J. Hizanidis, A. Balanov, A. Amann, and E. Schöll, Phys. Rev. Lett. **96**, 244104 (2006).
[11] J. P. Keener and J. Sneyd, *Mathematical Physiology* (Springer, New York, 1998).
[12] L. L. Bonilla, J. Phys. Condens. Matter **14**, R341 (2002).
[13] L. L. Bonilla and H. T. Grahn, Rep. Prog. Phys. **68**, 577 (2005).
[14] K. J. Luo, H. T. Grahn, and K. H. Ploog, Phys. Rev. B **57**, R6838 (1998).
[15] A. Amann, A. Wacker, L. L. Bonilla, and E. Schöll, Phys. Rev. E **63**, 066207 (2001).
[16] Y. Y. Huang, H. Qin, W. Li, S. L. Lu, J. R. Dong, H. T. Grahn, and Y. H. Zhang, Europhys. Lett. **105**, 47005 (2014).
[17] Y. Y. Huang, W. Li, W. Q. Ma, H. Qin, and Y. H. Zhang, Chin. Sci. Bull. **57**, 2070 (2012).
[18] W. Li, I. Reidler, Y. Aviad, Y. Y. Huang, H. Song, Y. H. Zhang, M. Rosenbluh, and I. Kanter, Phys. Rev. Lett. **111**, 044102 (2013).
[19] Y. Y. Huang, W. Li, W. Q. Ma, H. Qin, H. T. Grahn, and Y. H. Zhang, Appl. Phys. Lett. **102**, 242107 (2013).
[20] Z. Z. Yin, H. L. Song, Y. H. Zhang, M. Ruiz-Garcia, M. Carretero, L. L. Bonilla, K. Biermann, and H. T. Grahn, Phys. Rev. E **95**, 012218 (2017).
[21] M. Alvaro, M. Carretero, and L. L. Bonilla, Europhys. Lett. **107**, 37002 (2014).
[22] L. L. Bonilla, M. Alvaro, and M. Carretero, J. Math. Ind. **7**, 1 (2017).
[23] M. Ruiz-Garcia, J. Essen, M. Carretero, L. L. Bonilla, and B. Birnir, Phys. Rev. B **95**, 085204 (2017).
[24] J. Essen, M. Ruiz-Garcia, I. Jenkins, M. Carretero, L. L. Bonilla, and B. Birnir, Chaos **28**, 043107 (2018).
[25] Z. Z. Shao, Z. Z. Yin, H. L. Song, W. Liu, X. J. Li, J. Zhu, K. Biermann, L. L. Bonilla, H. T. Grahn, and Y. H. Zhang, following Letter, Phys. Rev. Lett. **121**, 086806 (2018).

[26] L. L. Bonilla, J. Galán, J. A. Cuesta, F. C. Martínez, and J. M. Molera, Phys. Rev. B **50**, 8644 (1994).
[27] L. L. Bonilla, G. Platero, and D. Sánchez, Phys. Rev. B **62**, 2786 (2000).
[28] See Supplemental Material at http://link.aps.org/supplemental/10.1103/PhysRevLett.121.086805 for description of the model, phase diagram of contact conductivity versus dc voltage, technical details about the critical total current, a movie related to Fig. 3, and two figures related to the stochastic resonance.
[29] H. Kroemer, IEEE Trans. Electron Devices **15**, 819 (1968).
[30] S. H. Strogatz, *Nonlinear Dynamics and Chaos* (Addison-Wesley, Reading, MA, 1994), Sec. 12.4.
[31] S. Mallat, *A Wavelet Tour of Signal Processing: The Sparse Way*, 3rd ed. (Academic, Burlington, MA 2008).